Accuracy of Pressure Sensitive Paint

AIAA Journal, Vol. 39, No.1, January 2001

Tianshu Liu[†]

† Research Scientist, NASA Langley Research Center

Model Systems Branch, MS 238

Hampton, VA 23681-2199, Member AIAA

and

M. Guille[*] and J. P. Sullivan[‡]

* Research Assistant, School of Aeronautics and Astronautics

Purdue University, West Lafayette, IN 47906, Student Member AIAA

‡ Professor, School of Aeronautics and Astronautics

Purdue University, West Lafayette, IN 47906, Member AIAA

Abstract

Uncertainty in pressure sensitive paint (PSP) measurement is investigated from a standpoint of system modeling. A functional relation between the imaging system output and luminescent emission from PSP is obtained based on studies of radiative energy transports in PSP and photodetector response to luminescence. This relation provides insights into physical origins of various elemental error sources and allows estimate of the total PSP measurement uncertainty contributed by the elemental errors. The elemental errors and their sensitivity coefficients in the error propagation equation are evaluated. Useful formulas are given for the minimum pressure uncertainty that PSP can possibly achieve and the upper bounds of the elemental errors to meet required pressure accuracy. An instructive example of a Joukowsky airfoil in subsonic flows is given to illustrate uncertainty estimates in PSP measurements.

Introduction

Pressure sensitive paint (PSP) is an optical technique for measuring surface pressure distributions on wind tunnel models [1-3]. Compared with conventional techniques such as pressure taps, PSP provides a non-contact way to obtain full-field measurements of surface pressure with much higher spatial resolution. Due to oxygen quenching of luminescence, luminescent intensity (I) emitted from PSP is related to air pressure (P) by the Stern-Volmer equation

$$\frac{I_0}{I} = 1 + K_p P, \tag{1}$$

where I_0 is the luminescent intensity in the absence of oxygen and K_p is the Stern-Volmer constant. Hence, air pressure can be determined by detecting the luminescent intensity of PSP. Since I_0 is not known in wind tunnel testing, experimental aerodynamicists often use another version of the Stern-Volmer equation

$$\frac{I_{ref}}{I} = A(T) + B(T)\frac{P}{P_{ref}}, \tag{2}$$

where I_{ref} and P_{ref} are the reference luminescent intensity and pressure at a known temperature, respectively. The coefficients *A(T)* and *B(T),* also called the Stern-Volmer constants, are related to the coefficient K_p by $B(T)/A(T) = K_p P_{ref}$. Obviously, a constraint is $A(T_{ref}) + B(T_{ref}) = 1$, where T_{ref} is a reference temperature. The Stern-Volmer equation (2) and its extended forms have been widely used as operational calibration relations for PSP measurements in aerodynamic tests. The Stern-Volmer coefficients *A(T)* and *B(T)* are temperature-dependent because temperature affects both non-radiative deactivation and oxygen diffusion in a polymer. The Stern-Volmer coefficients *A(T)* and *B(T)* can be approximately expressed as a linear function of temperature

$$A(T) \approx A(T_{ref})\left[1 + \frac{E_{nr}}{RT_{ref}}\left(\frac{T - T_{ref}}{T_{ref}}\right)\right] \text{ and } B(T) \approx B(T_{ref})\left[1 + \frac{E_p}{RT_{ref}}\left(\frac{T - T_{ref}}{T_{ref}}\right)\right], \tag{3}$$

where E_{nr} is the Arrhenius activation energy for the non-radiative process, E_p is the activation energy for oxygen diffusion, and R is the universal gas constant. Eq. (3) implies that the temperature dependence of *A(T)* is mainly due to the thermal quenching as temperature sensitive paint (TSP) while *B(T)* is related to the temperature dependence of the oxygen diffusivity in a polymer. For a typical PSP (Bath Ruth + silica gel in GE RTV 118), the coefficients in Eq. (3) are $A(T_{ref}) = 0.13$, $B(T_{ref}) = 0.87$, $E_{nr}/RT_{ref} = 2.82$, and $E_p/RT_{ref} = 4.32$ over a temperature range from $293K$ to $333K$, where the reference temperature is $T_{ref} = 298K$.

Uncertainty estimates for PSP measurements are highly desirable. Based on the Stern-Volmer equation, Sajben [4] investigated error sources contributing to the uncertainty of PSP measurements. He found that the uncertainty strongly depends on flow conditions and surface temperature

significantly affects the final measurement result. Oglesby *et al.* [5] presented an analysis of intrinsic limits of the Stern-Volmer relation to achievable sensitivity and accuracy. Mendoza [6, 7] studied CCD camera noise and its effect on PSP measurement and suggested the limiting Mach number for quantitative PSP measurements. Relevant issues of PSP uncertainty were also addressed in other literature [1,3,8]. On the other hand, Cattafesta *et al.* [9] gave uncertainty estimates for temperature sensitive paint (TSP) measurements with CCD cameras.

The Stern-Volmer equation (1) or (2) describes a generic relationship between air pressure and luminescent intensity. However, a complete analysis of PSP measurement uncertainty requires a more specific relation between air pressure and imaging system's output that depends on various system elements such as paint, photodetector, optical filters, and illumination sources. In this paper, solving the transport equations of radiative energy and modeling an imaging system, we obtain a functional relation between the imaging system's output and various system parameters such as the performance parameters of the optical system and the physical properties of PSP. Based on this relation, a sensitivity analysis is given to evaluate the major elemental error sources and total uncertainty in PSP measurements. The minimum pressure difference that PSP can resolve is derived and the upper bounds of the elemental errors for required pressure accuracy are estimated. A sample uncertainty analysis for subsonic flows over a Joukowsky airfoil is given to illustrate some issues in PSP measurements.

Luminescent Radiation and Photodetetor Response

Luminescent radiation from a PSP layer on a surface involves two major physical processes. The first process is absorption of an excitation light through the PSP layer. The incident excitation light with a wavelength λ_1 is absorbed when traveling in the layer, and is reflected and scattered back to the layer at the wall surface. The second is luminescent radiation that is an absorbing-

emitting process in the layer. After luminescent molecules in the layer are excited by the excitation light, they emit luminescence with a longer wavelength λ_2. Figure 1 illustrates absorption and surface reflection/scattering of an excitation light and radiation of luminescence in a PSP layer. In general, the illumination and emission processes in a PSP layer can be described by the transport equations of radiative energy [10,11]. When strong scattering and reflection occur only at the wall surface, the luminescent intensity emitted from a PSP layer in plane geometry can be analytically determined by solving the transport equations of radiative energy (see Appendix). When the PSP layer is optically thin, the outgoing luminescent energy flow rate $Q^+_{\lambda_2}$ (energy/time/wavelength) on an area element A_s of the PSP paint surface is

$$Q^+_{\lambda_2} = \beta_{\lambda_1} h \Phi(P,T) q_0 \, E_{\lambda_2}(\lambda_2) \, K_1 < M > A_s \Omega \,, \tag{4}$$

where Ω is the solid angle, $< M >$ is the coefficient representing the effects of reflection and scattering of the luminescent light at the wall, β_{λ_1} is the extinction coefficient of the PSP medium for the excitation light, h is the paint layer thickness, $\Phi(P,T)$ is the luminescent quantum yield that depends on air pressure and temperature, q_0 is the excitation light flux, and $E_{\lambda_2}(\lambda_2)$ is the luminescence spectrum. The term K_1 represents the combined effect of the optical filter for the excitation light, excitation light scattering, and direction of the incident excitation light. Here, the extinction coefficient $\beta_{\lambda_1} = \varepsilon_{\lambda_1} c$ is a product of the molar absorptivity ε_{λ_1} and luminescent molecule concentration c. When the PSP layer is optically thick, $Q^+_{\lambda_2}$ is a non-linear function of the paint thickness and extinction coefficients. Nevertheless, uncertainty analysis in this case is essentially the same as that for an optically thin PSP layer.

Consider an optical detector system (e.g. CCD camera) shown in Fig. 2. The detector output depends on not only the outgoing luminescent energy flow rate $Q^{+}_{\lambda_2}$, but also the performance parameters of the optical system. In Appendix, we obtain an expression for the output of the detector

$$V = G\frac{\pi}{4}\frac{A_I}{F^2(1+M_{op})^2}\beta_{\lambda_1} h\Phi(P,T)q_0\ K_1 K_2 \tag{5}$$

where V is the output of the detector, G is the system's gain, A_I is the image area, $F = fl / D$ is the f-number, $M_{op} = R_2 / R_1$ is the optical magnification, fl is the system's effective focal length, D is the aperture diameter, R_1 is the distance between the lens and the source area (e.g. model surface), and R_2 is the distance between the lens and the sensor. Physically, the term K_2 represents the combined effect of the optical filter for the luminescent light, luminescent light scattering, and system response to the luminescent light (see Appendix).

Modeling of PSP Measurement System

The detector output is

$$V = \Pi_c \Pi_f\ \beta_{\lambda_1} h q_0\ \Phi(P,T). \tag{6}$$

The parameters Π_c and Π_f are $\Pi_c = (\pi/4)G A_I [F^2(1+M_{op})^2]^{-1}$ and $\Pi_f = K_1 K_2$, which are related to the imaging system performance and filter parameters, respectively. The quantum yield $\Phi(P,T)$ is described by $\Phi(P,T) = k_r /(k_r + k_{nr} + k_q[O_2])$, where k_r is the radiative rate constant, k_{nr} is the non-radiative deactivation rate constant, k_q is the quenching rate constant, and $[O_2]$ is the oxygen concentration. This relation reflects the competition among the radiation, non-radiative deactivation and quenching processes. The concentration of oxygen is related to air pressure P by Henry's law $[O_2] = S\,a\,P$, where S is the solubility of oxygen and a is the volume fraction of

oxygen in air. In PSP applications, the intensity-ratio method is currently used as a typical procedure to eliminate the effects of spatial variation in illumination, paint thickness, and molecule concentration. When a ratio between the wind-on and reference wind-off images is taken, air pressure P can be expressed in terms of the system's outputs and other variables

$$P = U_1 \frac{V_{ref}(t, \boldsymbol{x})}{V(t', \boldsymbol{x}')} \frac{P_{ref}}{B(T)} - \frac{A(T) P_{ref}}{B(T)}. \tag{7}$$

The factor U_1 is

$$U_1 = \frac{\Pi_c}{\Pi_{c\,ref}} \frac{\Pi_f}{\Pi_{f\,ref}} \frac{h(\boldsymbol{x}')}{h_{ref}(\boldsymbol{x})} \frac{c(\boldsymbol{x}')}{c_{ref}(\boldsymbol{x})} \frac{q_0(t', \boldsymbol{X}')}{q_{0\,ref}(t, \boldsymbol{X})},$$

where $\boldsymbol{x} = (x, y)^T$ and $\boldsymbol{x}' = (x', y')^T$ are the coordinates in the wind-off and wind-on images, respectively, $\boldsymbol{X} = (X, Y, Z)^T$ and $\boldsymbol{X}' = (X', Y', Z')^T$ are the object space coordinates in the wind-off and wind-on cases, respectively, and t and t' are the instants at which the wind-off and wind-on images are taken, respectively. Here the paint thickness and dye concentration are expressed as a function of $\boldsymbol{x}$ rather than $\boldsymbol{X}$ because image registration errors are more easily treated in the image plane. In fact, $\boldsymbol{x}$ and $\boldsymbol{X}$ are related through the perspective collinearity equations in photogrammetry.

In order to separate complicated coupling between the temporal and spatial variations of the variables, some terms in (7) can be further decomposed when a small model deformation and a short time interval are considered. The wind-on image coordinates can be expressed as a superposition of the wind-off coordinates and displacement vector, i.e., $\boldsymbol{x}' = \boldsymbol{x} + \Delta\boldsymbol{x}$. Similarly, the time decomposition is $t' = t + \Delta t$. For small $\Delta\boldsymbol{x}$ and Δt, the ratio of the images can be separated into two factors, $V_{ref}(t, \boldsymbol{x})/V(t', \boldsymbol{x}') \approx D_t(\Delta t)\, D_x(\Delta\boldsymbol{x}) V_{ref}(t, \boldsymbol{x})/V(t, \boldsymbol{x})$, where the factor

$D_t(\Delta t) = 1 - (\partial V / \partial t)(\Delta t)/V$ and $D_x(\Delta \boldsymbol{x}) = 1 - (\nabla V) \bullet (\Delta \boldsymbol{x})/V$ represent the effects of the temporal and spatial changes of the luminescent intensity, respectively. The temporal change of the luminescent intensity is mainly caused by photodegradation and sedimentation of dusts and oil droplets on a surface. The spatial intensity change is due to model deformation. In the same fashion, the excitation light flux is decomposed into $q_0(t', \boldsymbol{X'})/q_{0\,ref}(t, \boldsymbol{X}) \approx D_{q0}(\Delta t) q_0(t, \boldsymbol{X'})/q_{0\,ref}(t, \boldsymbol{X})$, where the factor $D_{q0}(\Delta t) = 1 + (\partial q_0 / \partial t)(\Delta t)/q_{0\,ref}$ reflects the temporal variation in the excitation light flux. The use of the above estimates yields the modified Stern-Volmer equation

$$P = U_2 \frac{V_{ref}(t, \boldsymbol{x})}{V(t, \boldsymbol{x})} \frac{P_{ref}}{B(T)} - \frac{A(T) P_{ref}}{B(T)}. \tag{8}$$

where

$$U_2 = D_t(\Delta t) D_x(\Delta \boldsymbol{x}) D_{q0}(\Delta t) \frac{\Pi_c}{\Pi_{c\,ref}} \frac{\Pi_f}{\Pi_{f\,ref}} \frac{h(\boldsymbol{x'})}{h_{ref}(\boldsymbol{x})} \frac{c(\boldsymbol{x'})}{c_{ref}(\boldsymbol{x})} \frac{q_0(t, \boldsymbol{X'})}{q_{0\,ref}(t, \boldsymbol{X})}.$$

Without model motion ($\boldsymbol{x'} = \boldsymbol{x}$ and $\boldsymbol{X'} = \boldsymbol{X}$) and temporal illumination fluctuation, the factor U_2 is unity and then Eq. (8) recovers the generic Stern-Volmer equation. However, unlike the generic Stern-Volmer equation used in previous PSP uncertainty estimates, Eq. (8) is a general relation that includes the effects of model deformation, spectral variability, and temporal variations in both illumination and luminescence. This relation allows a more complete uncertainty analysis and a clearer understanding of how these variables contribute the total uncertainty in PSP measurements.

Error Propagation, Sensitivity and Total Uncertainty

According to general uncertainty analysis formalism [12,13], the total uncertainty of pressure *P* is described by the error propagation equation

$$\frac{var(P)}{P^2} = \sum_{i,j=1}^{M} S_i S_j \rho_{ij} \frac{[var(\zeta_i)var(\zeta_j)]^{1/2}}{\zeta_i \zeta_j}, \tag{9}$$

where $\rho_{ij} = cov(\zeta_i \zeta_j)/[var(\zeta_i)var(\zeta_j)]^{1/2}$ is the correlation coefficient between the variables ζ_i and ζ_j, $var(\zeta_i) = <\Delta\zeta_i^2>$ and $cov(\zeta_i \zeta_j) = <\Delta\zeta_i \Delta\zeta_j>$ are the variance and covariance, respectively, and the notation $<>$ denotes the statistical assemble average. Here the variables $\{\zeta_i, i = 1 \cdots M\}$ denote a set of the parameters $D_t(\Delta t)$, $D_x(\Delta \mathbf{x})$, $D_{q0}(\Delta t)$, V, V_{ref}, $\Pi_c/\Pi_{c\,ref}$, $\Pi_f/\Pi_{f\,ref}$, h/h_{ref}, c/c_{ref}, $q_0/q_{0\,ref}$, P_{ref}, T, *A*, and *B*. The sensitivity coefficients S_i are defined as $S_i = (\zeta_i/P)(\partial P/\partial \zeta_i)$. Eq. (9) becomes particularly simple when the cross-correlation coefficients between the variables vanish ($\rho_{ij} = 0, i \neq j$). Table I lists the sensitivity coefficients, the elemental errors and their physical origins. Many sensitivity coefficients are proportional to a factor $1 + [A(T)/B(T)] / (P/P_{ref})$. For Bath Ruth + silica-gel in GE RTV 118, Figure 3 shows the factor $1 + [A(T)/B(T)] / (P/P_{ref})$ as a function of P/P_{ref} for different temperatures. This factor is only slightly changed by temperature. The temperature sensitivity coefficient is $S_T = -T[B'(T) + A'(T) P_{ref}/P]/B(T)$, where the prime denotes differentiation. Figure 4 shows the absolute value of S_T as a function of P/P_{ref} at different temperatures. As long as the elemental errors are evaluated, the total uncertainty in pressure can be calculated using Eq. (9). The major elemental error sources will be discussed below.

Elemental Error Sources

Photodetector noise and limiting pressure resolution

The uncertainties in the photodetector outputs V and V_{ref} are contributed from various noise sources in a photodetector (e.g. camera) such as photon shot noise, dark current shot noise, amplifier

noise, quantization noise, and pattern noise. When the dark current and pattern noise are subtracted and the noise floor is negligible, the detector noise is photon-shot-noise-limited. In this case, the signal-to-noise ratio (*SNR*) of the detector is $SNR = (V / G\hbar\nu B_d)^{1/2}$, where $\hbar$ is the Planck's constant [Js], ν is the frequency [s^{-1}], B_d is the electrical bandwidth [s^{-1}] of the detection electronics, G is the system's gain, and V is the detector output. The uncertainties in the outputs are $var(V) = VG\hbar\nu B_d$ and $var(V_{ref}) = V_{ref} G\hbar\nu B_d$. In the photon-shot-noise-limited case in which the error propagation equation contains only two terms related to V and V_{ref}, the uncertainty in P is

$$\frac{\Delta P}{P} = \left(\frac{G B_d \hbar \nu}{V_{ref}} \right)^{1/2} \left[1 + \frac{A(T)}{B(T)} \frac{P_{ref}}{P} \right] \left[1 + A(T) + B(T) \frac{P}{P_{ref}} \right]^{1/2}. \quad (10)$$

This relation holds for both non-imaging detectors and CCD. For a CCD camera, the first factor in the right-hand side of Eq. (10) can be simply expressed by the total number of photoelectrons collected over the integration time ($\propto 1/B_d$) $n_{pe} = V/(G\hbar\nu B_d)$. When the full-well capacity of a CCD is achieved, one obtains the minimum pressure difference that PSP can measure from a single frame of image

$$\frac{(\Delta P)_{min}}{P} = \frac{1}{\sqrt{(n_{pe\,ref})_{max}}} \left[1 + \frac{A(T)}{B(T)} \frac{P_{ref}}{P} \right] \left[1 + A(T) + B(T) \frac{P}{P_{ref}} \right]^{1/2}, \quad (11)$$

where $(n_{pe\,ref})_{max}$ is the full-well capacity of a CCD in reference conditions. When *N* images are averaged, the limiting pressure difference (11) is further reduced by a factor $N^{1/2}$. Eq. (11) provides an estimate for the noise-equivalent pressure resolution for a CCD camera. When $(n_{pe\,ref})_{max}$ is 500,000 electrons and Bath Ruth + silica-gel in GE RTV 118 is used, the minimum pressure uncertainty $(\Delta P)_{min} / P$ is shown in Fig. 5 as a function of P/P_{ref} for different temperatures. It is

indicated that an increasing temperature degrades the limiting pressure resolution. Figure 6 shows $\sqrt{(n_{pe\,ref})_{max}}(\Delta P)_{min}/P$ as a function of P/P_{ref} for different values of the Stern-Volmer coefficient $B(T)$. Clearly, a larger $B(T)$ leads to a smaller limiting pressure uncertainty $(\Delta P)_{min}/P$.

Errors induced by model deformation

Model deformation due to aerodynamic loads causes a displacement $\Delta\boldsymbol{x} = \boldsymbol{x}' - \boldsymbol{x}$ of the wind-on image relative to the wind-off image. This displacement leads to the deviations of $D_x(\Delta\boldsymbol{x})$, h/h_{ref}, c/c_{ref}, and $q_0/q_{0\,ref}$ in Eq. (8) from unity because the distributions of the luminescent intensity, paint thickness and dye concentration are not spatially homogeneous on a surface. After the image registration is applied to align the images, the estimated variances are $var[D_x(\Delta\boldsymbol{x})] \approx W(V)/V^2$, $var(h/h_{ref}) \approx W(h)/(h_{ref})^2$, and $var(c/c_{ref}) \approx W(c)/(c_{ref})^2$. The operator $W(\bullet)$ is defined as $W(\bullet) = (\partial/\partial x)^2\sigma_x^2 + (\partial/\partial y)^2\sigma_y^2$, where σ_x and σ_y are the standard deviations of least-squares estimation in the image registration.

The uncertainty in $q_0(\boldsymbol{X})/q_{0\,ref}(\boldsymbol{X}')$ is caused by a change in the illumination intensity on a model surface after the model moves with respect to the light sources. When a point on the model surface travels along the displacement vector $\Delta\boldsymbol{X} = \boldsymbol{X}' - \boldsymbol{X}$ in object space, the variance of $q_0/q_{0\,ref}$ is estimated by $var[q_0(\boldsymbol{X})/q_{0\,ref}(\boldsymbol{X}')] \approx (q_{0\,ref})^{-2}\left|(\nabla q_0)\bullet(\Delta\boldsymbol{X})\right|^2$. Consider a point light source with a light flux distribution $q_0(\boldsymbol{X} - \boldsymbol{X}_s) = \left|\boldsymbol{X} - \boldsymbol{X}_s\right|^{-n}$, where n is an exponent (normally n = 2) and $\left|\boldsymbol{X} - \boldsymbol{X}_s\right|$ is the distance between the point $\boldsymbol{X}$ on the model surface and the light source location $\boldsymbol{X}_s$. The variance of $q_0/q_{0\,ref}$ for the single point source is $var[q_0(\boldsymbol{X})/q_{0\,ref}(\boldsymbol{X}')]$

$= n^2 \left| \boldsymbol{X} - \boldsymbol{X}_s \right|^{-4} \left| (\boldsymbol{X} - \boldsymbol{X}_s) \bullet (\Delta \boldsymbol{X}) \right|^2$. The variance for multiple point light sources can be obtained based on the principle of superposition. In addition, model deformation leads to a small change in the distance between the model surface and the camera lens. The uncertainty in the camera performance parameters due to this change is $var(\Pi_c / \Pi_{c\,ref}) \approx [R_2/(R_1 + R_2)]^2 (\Delta R_1 / R_1)^2$, where R_1 is the distance between the lens and the model surface and R_2 is the distance between the lens and the sensor. For $R_1 >> R_2$, this error is very small.

Temperature effects

Since the luminescent intensity of PSP is intrinsically temperature-dependent, a temperature change on a model surface during wind tunnel runs results in a bias error in PSP measurement if the temperature effects are not corrected. Temperature also influences the total uncertainty of PSP measurement by altering the sensitivity coefficients of the variables in the error propagation equation. Hence, the surface temperature on a model must be known in order to correct the temperature effects of PSP. In general, the surface temperature distribution can be either measured by using temperature sensitive paint (TSP) or determined numerically by solving the energy equation in flows coupled with the heat conduction equation in the model. For a compressible boundary layer on an adiabatic wall, the adiabatic wall temperature T_{aw} can be estimated using a simple relation $T_{aw}/T_0 = [1 + r(\gamma - 1)M^2/2][1 + (\gamma - 1)M^2/2]^{-1}$, where r is the recovery factor for the boundary layer, T_0 is the total temperature, M is the local Mach number, and γ is the specific heat ratio.

PSP calibration errors

The uncertainties in determining the Stern-Volmer coefficients *A(T)* and *B(T)* are calibration errors. In *a priori* PSP calibration in a pressure chamber, the uncertainty is represented by the

standard deviation of data collected in replication tests. Because the tests in a pressure chamber are well controlled, *a priori* calibration result shows a small precision error. However, a significant bias error is usually found when the *a priori* calibration result is directly used for data reduction in wind tunnel tests. In contrast, *in-situ* calibration utilizes pressure tap data over a model surface to determine the Stern-Volmer coefficients. Because the *in-situ* calibration fits the local luminescent intensity to the pressure tap data, it can to some extent reduce bias errors such as the temperature effects and naturally achieves a better agreement with the pressure tap data.

Temporal variations in luminescence and illumination

For PSP measurements in steady flows, a temporal change in the luminescent intensity mainly results from the photodegradation and sedimentation of dusts and oil droplets on a model surface. The photodegradation of PSP may occur when there is a considerable exposure of PSP to the excitation light between the wind-off and wind-on measurements. Dusts and oil droplets in air sediment on a model surface during wind-tunnel runs. The resulting dust/oil layer absorbs both the excitation light and luminescent emission on the surface and thus causes a decrease of the luminescent intensity. The uncertainty in $D_t(\Delta t)$ due to these effects can be collectively characterized by the variance $var[D_t(\Delta t)] \approx [(\partial V / \partial t)(\Delta t)/V]^2$. Similarly, the uncertainty in $D_{q0}(\Delta t)$, which is produced by an unstable excitation light source, is described by $var[D_{q0}(\Delta t)] \approx [(\partial q_0 / \partial t)(\Delta t)/q_{0\,ref}]^2$.

Spectral variability and filter leakage

The uncertainty in $II_f / II_{f\,ref}$ is mainly attributed to the spectral variability in the illumination light and spectral leaking of the filters. The spectral variability between flashes of a xenon lamp has been observed [14]. The uncertainties in the absolute pressure and pressure coefficient due to the

flash spectral variability are 0.05 psi and 0.01, respectively. If the optical filters are not selected appropriately, a small portion of photons from the excitation light and ambient light may reach the detector through the filters. This spectral leakage produces an additional output to the luminescent signal.

Pressure mapping errors

The uncertainties in pressure mapping are related to the data reduction procedure in which PSP data in 2D images are mapped onto a model surface grid in 3D object space. They include errors in camera calibration and mapping onto a surface grid of a presumed rigid body. The camera calibration error is represented by the standard deviations σ_x and σ_y of the calculated target coordinates from the measured target coordinates in the image plane. Typically, a good camera calibration method gives the standard deviation of about 0.04 pixels. For a given PSP image, the pressure variance induced by the camera calibration error is $var(P) \approx (\partial P/\partial x)^2 \sigma_x^2 + (\partial P/\partial y)^2 \sigma_y^2$.

The pressure mapping onto a non-deformed surface grid leads to another deformation-related error since the model undergoes considerable deformation due to aerodynamic loads in wind tunnel tests. If a displacement vector of a point on the model surface in object space is $\Delta \boldsymbol{X} = \boldsymbol{X'} - \boldsymbol{X}$, the pressure variance induced by mapping onto a rigid body grid without correcting the deformation is $var(P) = \left| (\nabla P)_{surf} \bullet (\Delta \boldsymbol{X})_{surf} \right|^2$, where $(\nabla P)_{surf}$ is the pressure gradient on the surface and $(\Delta \boldsymbol{X})_{surf}$ is the component of the displacement vector projected on the surface. To eliminate this error, a deformed surface grid has to be generated for PSP mapping based on model deformation measurements [15].

Other error sources

Other error sources include self-illumination, paint intrusiveness, limiting time response, and induction effect. Self-illumination is a phenomenon that luminescence from one part of a model surface reflects to another surface, thus distorting the observed luminescent intensity by superposing all the rays reflected from other points. It often occurs on surfaces of neighbor components of a complex model. Ruyten [16] discussed this problem and gave a numerical correction procedure for self-illumination. Paint layer with a non-homogenous thickness modifies the shape of a model such that the surface pressure distribution may be changed. Hence, this paint intrusiveness to flows should be considered as an error source in PSP measurements. In PSP applications in unsteady flows, the limiting time response of PSP imposes an additional restriction on the accuracy of PSP measurement. The time response of PSP is mainly determined by oxygen diffusion process through the PSP layer [17]. Another problem related to the time response is the 'induction effect' defined as an increase in luminescence during the first few minutes of illumination. This effect has been observed with certain paints and the photochemical process behind it has been explained by Gouterman [18].

Allowable Upper Bounds of Elemental Errors

In the design of PSP experiments, we need to give the allowable upper bounds of the elemental errors for required pressure accuracy. This is an optimization problem subject to constraints. In matrix notations, Eq. (9) is expressed as $\sigma_P^2 = \boldsymbol{\sigma}^T \boldsymbol{A}\, \boldsymbol{\sigma}$, where $\sigma_P^2 = var(P)/P^2$, $A_{ij} = S_i S_j \rho_{ij}$, and $\sigma_i = [\, var(\zeta_i)\,]^{1/2} / \zeta_i$. For a required pressure uncertainty σ_P, we look for a vector $\boldsymbol{\sigma_{up}}$ to maximize an objective function $H = \boldsymbol{W}^T \boldsymbol{\sigma}$, where $\boldsymbol{W}$ is the weighting vector. The vector $\boldsymbol{\sigma_{up}}$ gives the upper bounds of the elemental errors for a given pressure uncertainty σ_P. The use of the

Lagrange multiplier method requires $\overline{H} = \boldsymbol{W}^{\boldsymbol{T}} \boldsymbol{\sigma} + \lambda(\sigma_P^2 - \boldsymbol{\sigma}^{\boldsymbol{T}} \boldsymbol{A} \boldsymbol{\sigma})$ to be maximal, where λ is the Lagrange multiplier. The solution to this optimization problem gives the upper bounds

$$\boldsymbol{\sigma}_{\boldsymbol{up}} = \frac{\boldsymbol{A}^{-1} \boldsymbol{W}}{(\boldsymbol{W}^{\boldsymbol{T}} \boldsymbol{A}^{-1} \boldsymbol{W})^{1/2}} \sigma_P . \tag{12}$$

For the uncorrelated variables with $\rho_{ij} = 0 \ (i \neq j)$, Eq. (12) reduces to

$$(\sigma_i)_{\boldsymbol{up}} = S_i^{-2} W_i \sigma_P \left(\sum_k S_k^{-2} W_k^2 \right)^{-1/2} . \tag{13}$$

When the weighting factors W_i equal the absolute values of the sensitivity coefficients $|S_i|$, the upper bounds can be expressed in a very simple form

$$(\sigma_i)_{\boldsymbol{up}} / \sigma_P = N_V^{-1/2} \left| S_i \right|^{-1}, \qquad (i = 1,2,\cdots,N_V) \tag{14}$$

where N_V is the total number of the variables or the elemental error sources. The relation (14) clearly indicates that the allowable upper bounds of the elemental uncertainties are inversely proportional to the sensitivity coefficients and the square root of the total number of the elemental error sources. Figure 7 shows a distribution of the upper bounds of 15 variables for Bath Ruth + silica-gel in GE RTV 118 at $P / P_{ref} = 0.8$ and $T = 293K$. Clearly, the allowable upper bound for temperature is much lower than others. Therefore, the temperature effcts must be tightly controlled in order to achieve the required pressure accuracy.

PSP Uncertainty Estimates on a Joukowsky Airfoil in Subsonic Flows

Hypothetical PSP measurements on a Joukowsky airfoil in subsonic flows are considered to illustrate how to estimate the elemental errors and the total uncertainty by using the techniques developed above. The airfoil and incompressible potential flows around it are generated by using the Joukowsky transform. The pressure coefficients C_p on the airfoil in the corresponding

compressible flows are obtained by using the Karman and Tsien rule. Figure 8 shows typical distributions of the pressure coefficient and adiabatic wall temperature on the Joukowsky airfoil at Mach 0.5.

Presumably, Bath Ruth + silica-gel in GE RTV 118 is used, which has the Stern-Volmer coefficients $A(T) \approx 0.13\,[1 + 2.82(T - T_{ref})/T_{ref}]$ and $B(T) \approx 0.87\,[1 + 4.32(T - T_{ref})/T_{ref}]$ ($293K < T < 333K$). The uncertainties in *a priori* PSP calibration are $\Delta A/A = \Delta B/B = 1\%$. Assume that the spatial changes of the paint thickness and dye concentration in the image plane are 0.5%/pixel and 0.1%/pixel, respectively. The rate of the photodegradation of the paint is 0.5%/hour for a given excitation level and the exposure time of the paint is 60 seconds between the wind-off and wind-on images. The rate of reduction of the luminescent intensity due to dust/oil sedimentation on the surface is assumed to be 0.5%/hour.

In an object-space coordinate system whose origin is at the leading edge of the airfoil, four light sources for illuminating PSP are placed at the locations $\boldsymbol{X}_{s1} = (-\bar{c}, 3\bar{c})$, $\boldsymbol{X}_{s2} = (2\bar{c}, 3\bar{c})$, $\boldsymbol{X}_{s3} = (-\bar{c}, -3\bar{c})$, and $\boldsymbol{X}_{s4} = (2\bar{c}, -3\bar{c})$, where $\bar{c}$ is the chord of the airfoil. For the light sources with unit strength, the illumination flux distributions on the upper and lower surfaces are, respectively, $(q_0)_{up} = |\boldsymbol{X}_{up} - \boldsymbol{X}_{s1}|^{-2} + |\boldsymbol{X}_{up} - \boldsymbol{X}_{s2}|^{-2}$ and $(q_0)_{low} = |\boldsymbol{X}_{low} - \boldsymbol{X}_{s3}|^{-2} + |\boldsymbol{X}_{low} - \boldsymbol{X}_{s4}|^{-2}$, where $\boldsymbol{X}_{up}$ and $\boldsymbol{X}_{low}$ are the coordinates of the upper and lower surfaces of the airfoil, respectively. The temporal variation of irradiance of the lights is assumed to be 1%/hour. It is also assumed that the spectral leakage of the optical filters for the lights and cameras is 0.3%. Two cameras, viewing the upper surface and lower surface respectively, are located at $(\bar{c}/2, 4\bar{c})$ and $(\bar{c}/2, -4\bar{c})$.

The uncertainty associated with the shot noise can be estimated by using Eq. (10). Assume that the full-well capacity of $(n_{pe})_{max} = 350{,}000$ electrons of a CCD camera is utilized. The numbers of photoelectrons collected in the CCD camera are mainly proportional to the distributions of the illumination fields on the model surfaces. Thus, the photoelectrons on the upper and lower surfaces are estimated by $(n_{pe})_{up} = (n_{pe})_{max}(q_0)_{up} / max[(q_0)_{up}]$ and $(n_{pe})_{low} = (n_{pe})_{max}(q_0)_{low} / max[(q_0)_{low}]$. Combination of these estimates and Eq. (10) can give the shot-noise-generated uncertainty distributions on the surfaces.

Movement of the airfoil produced by aerodynamic loads can be expressed by a superposition of local rotation (twist) and translation. The transformation between the non-moved and moved surface coordinates $\boldsymbol{X} = (X, Y)^T$ and $\boldsymbol{X'} = (X', Y')^T$ is $\boldsymbol{X'} = \boldsymbol{R}(\theta_{twist})\boldsymbol{X} + \boldsymbol{T}$, where $\boldsymbol{R}(\theta_{twist})$ is the rotation matrix, θ_{twist} is the local wing twist, and $\boldsymbol{T}$ is the translation vector. Here, for $\theta_{twist} = -1^o$ and $\boldsymbol{T} = (0.001\bar{c}, 0.01\bar{c})^T$, the uncertainty in $q_0(\boldsymbol{X})/q_{0\,ref}(\boldsymbol{X'})$ is estimated by $var[q_0(\boldsymbol{X})/q_{0\,ref}(\boldsymbol{X'})] \approx (q_{0\,ref})^{-2}\left|(\nabla q_0)\bullet(\Delta \boldsymbol{X})\right|^2$, where the displacement vector is $\Delta\boldsymbol{X} = \boldsymbol{X'} - \boldsymbol{X}$. The pressure variance associated with mapping onto a rigid body grid without correcting the deformation is estimated by $var(P) = \left|(\nabla P)_{surf} \bullet (\Delta \boldsymbol{X})_{surf}\right|^2$, where $(\nabla P)_{surf}$ is the pressure gradient on the surface and $(\Delta \boldsymbol{X})_{\boldsymbol{surf}} = (\boldsymbol{X'} - \boldsymbol{X})_{\boldsymbol{surf}}$ is the component of the displacement vector projected on the surface.

To estimate the temperature effects, an adiabatic model is considered at which the wall temperature T_{aw} is $T_{aw}/T_0 = [1 + r(\gamma - 1)M^2/2][1 + (\gamma - 1)M^2/2]^{-1}$. The recovery factor is $r = 0.843$ for a laminar boundary layer. Assuming that the reference temperature T_{ref} equals to the total

temperature $T_0 = 293K$, one can calculate the temperature difference $\Delta T = T_{aw} - T_{ref}$ between the wind-on and wind-off cases (Fig. 8).

The total uncertainty in air pressure *P* is estimated by substituting all the elemental errors into Eq. (9). Figure 9 shows the pressure uncertainty distributions on the upper and lower surfaces of the airfoil for different freestream Mach numbers. It is indicated that the temperature effects of PSP dominate the uncertainty of PSP measurement in an adiabatic wall. The uncertainty becomes larger and larger as Mach number increases since the adiabatic wall temperature increases. The local pressure uncertainty on the upper surface is as high as 50% at one location for Mach = 0.7, which is caused by the local surface temperature change of about 6 degrees. In order to compare the PSP uncertainty with the pressure variation on the airfoil, a maximum relative pressure variation on the airfoil is defined as $max\left|\Delta P\right|_{surf} / P_\infty = 0.5\,\gamma M_\infty^2\, max\left|\Delta C_p\right|$. Figure 10 shows the maximum relative pressure variation $max\left|\Delta P\right|_{surf} / P_\infty$ along with the chord-averaged PSP uncertainty $<(\Delta P/P)_{PSP}>_{aw}$ on the adiabatic airfoil at Mach numbers ranging from 0.05 to 0.7. The uncertainty $<(\Delta P/P)_{PSP}>_{\Delta T=0}$ without the temperature effects is also plotted in Fig. 10, which is mainly dominated by the *a priori* PSP calibration error $\Delta B/B = 1\%$ in this case. The curves $max\left|\Delta P\right|_{surf} / P_\infty$, $<(\Delta P/P)_{PSP}>_{aw}$ and $<(\Delta P/P)_{PSP}>_{\Delta T=0}$ intersect near Mach 0.1. When the PSP uncertainty exceeds the maximum pressure variation on the airfoil, the pressure distribution on the airfoil cannot be measured by PSP. In general, because of a smaller temperature change on a non-adiabatic wall, the PSP uncertainty for a real wind tunnel model falls into the shadowed region confined by $<(\Delta P/P)_{PSP}>_{aw}$ and $<(\Delta P/P)_{PSP}>_{\Delta T=0}$ (see Fig. 10). The PSP uncertainty associated with the shot noise $<(\Delta P/P)_{PSP}>_{ShotNoise}$ is also plotted in Fig. 10. The intersection

between $max|\Delta P|_{surf} / P_\infty$ and $<(\Delta P/P)_{PSP}>_{ShotNoise}$ gives the limiting low Mach number (~ 0.06) for PSP application. The uncertainties in the lift (F_L) and pitching moment (M_c) can also be calculated from the PSP uncertainty distribution on the surface. Figure 11 shows the uncertainties in the lift and pitching moment relative to the leading edge for the Joukowsky airfoil at different Mach numbers when the angle of attack is 4 degrees. The uncertainties in the lift and moment decrease monotonously as Mach number increases because the absolute values of the lift and moment rapidly increase with Mach number.

Conclusions

Based on more rigorous PSP system modeling, a general framework is built in which the physical origins of the elemental error sources are clearly identified and their contributions to the total uncertainty are systematically evaluated. For a required pressure uncertainty, the allowable upper bounds of the elemental errors are given by a simple formula, which are inversely proportional to the sensitivity coefficients. Among the major elemental error sources, for a typical PSP, temperature has the largest sensitivity coefficient and the lowest allowable upper bound of error in PSP measurements. Therefore, the temperature effects must be corrected in order to obtain quantitative pressure results. The minimum pressure uncertainty limited by the photon-shot-noise can be described by an analytical expression, which is related to the Stern-Volmer coefficients, local air pressure and the number of photoelectrons. The shot-noise-limited PSP uncertainty increases with temperature and decreases as the Stern-Volmer coefficient *B(T)* increases. The sample uncertainty analysis on a Joukowsky airfoil in subsonic flows further confirms that the temperature effects dominate the PSP measurement uncertainty. It is enlightening to compare the uncertainties in several different conditions (on the adiabatic wall, without the temperature effects, and in the

shot-noise-limited case) with the maximum relative pressure change on the surface as a function of freestream Mach number. This comparison not only shows the uncertainties relative to the surface pressure change, but also gives the limiting low Mach number for PSP measurements.

Acknowledgments

The authors would like to thank the reviewers for their constructive comments.

References

[1] Crites, B. C., "Measurement Techniques — Pressure Sensitive Paint Technique," Lecture Series 1993-05, von Karman Institute for Fluid Dynamics, 1993.

[2] McLachlan, B. G. and Bell, J. H., "Pressure-Sensitive Paint in Aerodynamic Testing," *Experimental Thermal and Fluid Science*, 10, 1995, pp. 470-485.

[3] Liu, T., Campbell, B. T., Burns, S. P. and Sullivan, J. P., "Temperature- and Pressure-Sensitive Luminescent Paints in Aerodynamics," *Applied Mechanics Reviews*, Vol. 50, No. 4, 1997, pp. 227-246.

[4] Sajben, M., "Uncertainty Estimates for Pressure Sensitive Paint Measurements," *AIAA J.*, Vol. 31, No. 11, 1993, pp. 2105-2110.

[5] Oglesby, D. M., Puram, C. K. and Upchurch, B. T., "Optimization of Measurements with Pressure Sensitive Paints," NASA TM 4695, 1995.

[6] Mendoza, D. R., "An Analysis of CCD Camera Noise and its Effect on Pressure Sensitive Paint Instrumentation System Signal-to-Noise Ratio," ICIASF '97 Record, International Congress on Instrumentation in Aerospace Simulation Facilities, Pacific Grove, CA, September 29-October 2, 1997, pp. 22-29.

[7] Mendoza, D. R., "Limiting Mach Number for Quantitative Pressure-Sensitive Paint Measurements," *AIAA J.*, Vol. 35, No. 7, 1997, pp. 1240-1241.

[8] Morris, M. J., Benne, M. E., Crites, R. C. and Donovan, J. F., "Aerodynamics Measurements Based on Photoluminescence," AIAA Paper 93-0175, Jan. 1993.

[9] Cattafesta, L., Liu, T., and Sullivan, J., "Uncertainty Estimates for Temperature Sensitive Paint Measurements with CCD Cameras," *AIAA J.*, Vol. 36, No. 11, 1998, pp. 2102-2108.

[10] Pomraning, G. C., "Radiation Hydrodynamics," Pergamon Press, New York, 1973, pp. 10-49.

[11] Modest, M. F., "Radiative Heat Transfer," McGraw-Hill, Inc., New York, 1993, pp. 295-320.

[12] Ronen, Y., "Uncertainty Analysis," CRC Press, Inc., Boca Raton, Florid, 1988, pp. 2-39.

[13] Bevington, P. R. and Robinson, D. K., "Data Reduction and Error Analysis for the Physical Sciences (Second Edition)," McGraw-Hill, Inc., New York, 1992, pp. 38-48.

[14] Possolo, A. and Maier, R., "Gauging Uncertainty in Pressure Measurement Due to Spectral Variability of Excitation Illumination," Proceeding of the Sixth Annual Pressure Sensitive Paint Workshop, The Boeing Company, Seattle, Washington, October 6-8, 1998, pp. 15-1 to 15-12.

[15] Liu, T., Radeztsky, R., Garg, S., and Cattafesta, L., "A Videogrammetric Model Deformation System and its Integration with Pressure Paint," AIAA Paper 99-0568, Jan. 1999.

[16] Ruyten, W. M., "Correcting Luminescent Paint Measurements for Self-Illumination," ICIASF '97 Record, International Congress on Instrumentation in Aerospace Simulation Facilities, Pacific Grove, CA, September 29-October 2, 1997, pp. 3-9.

[17] Carroll, B. F., Abbitt, J. D., Lukas, E. W. and Morris, M. J., "Step Response of Pressure Sensitive Paints," *AIAA J.*, Vol. 34, No. 3, 1996, pp. 521-526.

[18] Gouterman, M., "Oxygen Quenching of Luminescence of Pressure-Sensitive Paint for Wind Tunnel Research," *Journal of Chemical Education*, Vol. 74, No. 6, 1997, pp. 1-7.

Appendix: Luminescent Radiation from PSP and Photodetector Output

Luminescent radiation from a pressure sensitive paint (PSP) on a surface involves two major physical processes. The first process is absorption of an excitation light through a PSP layer. The second is luminescent radiation that is an absorbing-emitting process in the layer. These processes can be described by the transport equations of radiative energy [10, 11]. The luminescent intensity emitted from a PSP layer in plane geometry will be analytically determined by solving the transport equations and the corresponding photodetector output will be derived.

Excitation light

Consider a PSP layer with a thickness *h* on a wall (Figure 1). Suppose that PSP is not a scattering medium and scattering exists only at the wall surface. An incident excitation light beam with a wavelength λ_1 enters the layer. Without scattering and other sources for excitation energy, the incident light is attenuated by absorption through a PSP medium. In plane geometry where the radiative intensity is independent of the azimuthal angle, the intensity of the incident excitation light with λ_1 can be described by

$$\mu \frac{d I_{\lambda_1}^-}{dz} + \beta_{\lambda_1} I_{\lambda_1}^- = 0, \tag{A1}$$

where $I_{\lambda_1}^-$ is the incident excitation light intensity, $\mu = cos\theta$ is the cosine of the polar angle θ, and β_{λ_1} is the extinction coefficient of the PSP medium for the incident excitation light with λ_1. The extinction coefficient $\beta_{\lambda_1} = \varepsilon_{\lambda_1} c$ is a product of the molar absorptivity ε_{λ_1} and luminescent molecule concentration c. Here, the intensity is defined as radiative energy transferred per unit time, solid angle, spectral variable and area normal to the ray. The superscript '-' in $I_{\lambda_1}^-$ indicates the negative direction in which the light enters the layer. The incident angle θ ranges from $\pi/2$ to $3\pi/2$ ($-1 \le \mu \le 0$) (see Fig. 1). For the collimated excitation light, the boundary value for Eq. (A1) is the component penetrating into the PSP layer,

$$I_{\lambda_1}^-(z=h) = (1-\rho_{\lambda_1}^{ap}) q_0 E_{\lambda_1}(\lambda_1) \delta(\mu - \mu_{ex}), \tag{A2}$$

where q_0 and $E_{\lambda_1}(\lambda_1)$ are the radiative flux and spectrum of the incident excitation light, respectively, $\rho_{\lambda_1}^{ap}$ is the reflectivity of the air-PSP interface, μ_{ex} is the cosine of the incident angle of the excitation light, and $\delta(\mu)$ is the Dirac-delta function. The solution to Eq. (A1) is

$$I_{\lambda_1}^{-} = (1-\rho_{\lambda_1}^{ap})\, q_0\, E_{\lambda_1}(\lambda_1)\,\delta(\mu-\mu_{ex})\,exp[(\beta_{\lambda_1}/\mu)(h-z)]\,. \qquad (-1 \le \mu \le 0) \tag{A3}$$

This relation describes the decay of the incident excitation light intensity through the layer. The incident excitation light flux at the wall integrated over the ranges of θ from either π to $\pi/2$ or π to $3\pi/2$ is

$$q_{\lambda_1}^{-}(z=0) = -\int_{-1}^{0} I_{\lambda_1}^{-}(z=0)\,\mu\, d\mu \cong C_d\,(1-\rho_{\lambda_1}^{ap})\, q_0\, E_{\lambda_1}(\lambda_1), \tag{A4}$$

where C_d is the coefficient representing the directional effect of the excitation light, that is,

$$C_d = -\mu_{ex}\, exp(\beta_{\lambda_1} h/\mu_{ex})\,. \quad (-1 \le \mu_{ex} \le 0) \tag{A5}$$

When the incident excitation light impinges on the wall, the light reflects and re-enters into the layer. Without scattering source inside PSP, the intensity of the reflected and scattered light from the wall is described by

$$\mu \frac{d\, I_{\lambda_1}^{+}}{dz} + \beta_{\lambda_1}\, I_{\lambda_1}^{+} = 0, \tag{A6}$$

where $I_{\lambda_1}^{+}$ is the intensity in the positive direction emanating from the wall. As shown in Fig. 1, the range of μ is $0 \le \mu \le 1$ ($0 \le \theta \le \pi/2$ and $-\pi/2 \le \theta \le 0$) for the outgoing reflected and scattered light. The superscript '+' indicates the outgoing direction from the wall. For the wall that reflects diffusely, the boundary condition for Eq. (A6) is

$$I_{\lambda_1}^{+}(z=0) = \rho_{\lambda_1}^{wp}\, q_{\lambda_1}^{-}(z=0) = C_d\, \rho_{\lambda_1}^{wp}(1-\rho_{\lambda_1}^{ap})\, q_0\, E_{\lambda_1}(\lambda_1), \tag{A7}$$

where $\rho_{\lambda_1}^{wp}$ is the reflectivity of the wall-PSP interface for the excitation light. The solution to Eq. (A6) is

$$I_{\lambda_1}^{+} = C_d\, \rho_{\lambda_1}^{wp}(1-\rho_{\lambda_1}^{ap})\, q_0\, E_{\lambda_1}(\lambda_1)\, exp(-\beta_{\lambda_1} z/\mu). \qquad (0 \le \mu \le 1) \tag{A8}$$

At a point inside the PSP layer, the net excitation light flux is contributed by the incident and scattering light rays from all the possible directions. The net flux is calculated by adding the incident flux (integrated over $\theta = \pi \; to \; \pi/2$ and $\theta = \pi \; to \; 3\pi/2$) and scattering flux (integrated over $\theta = 0 \; to \; \pi/2$ and $\theta = 0 \; to \; -\pi/2$). The net flux is

$$(q_{\lambda_1})_{net} = -2\int_{-1}^{0} I_{\lambda_1}^{-} \mu \, d\mu - 2\int_{1}^{0} I_{\lambda_1}^{+} \mu d\mu$$
$$\cong C_d \, (1 - \rho_{\lambda_1}^{ap}) q_0 \, E_{\lambda_1}(\lambda_1)[\exp(-\beta_{\lambda_1} z/\mu_{ex}) + \rho_{\lambda_1}^{wp} \exp(-3\beta_{\lambda_1} z/2)] . \tag{A9}$$

Note that the derivation of Eq. (A9) uses the approximation of the exponential integral of third order, $E_3(x) \cong (1/2)\exp(-3x/2)$.

Luminescent emission

After luminescent molecules in PSP absorb the energy from the excitation light with a wavelength λ_1, they emit luminescence with a longer wavelength λ_2 due to the Stokes shift. Luminescent radiative transfer in PSP is an absorbing-emitting process. The luminescent light rays from the luminescent molecules radiate in both the inward and outward directions.

For the luminescent emission toward the wall, the luminescent intensity $I_{\lambda_2}^{-}$ can be described by

$$\mu \frac{d I_{\lambda_2}^{-}}{dz} + \beta_{\lambda_2} I_{\lambda_2}^{-} = S_{\lambda_2}(z), \quad (-1 \le \mu \le 0) \tag{A10}$$

where $S_{\lambda_2}(z)$ is the luminescent source term and the extinction coefficient $\beta_{\lambda_2} = \varepsilon_{\lambda_2} c$ is a product of the molar absorptivity ε_{λ_2} and luminescent molecule concentration c. The luminescent source term $S_{\lambda_2}(z)$ is assumed to be proportional to the extinction coefficient for the excitation light, the quantum yield, and the net excitation light flux filtered over a spectral range of absorption. A model for the luminescent source term is expressed as

$$S_{\lambda_2}(z) = \Phi(P,T) E_{\lambda_2}(\lambda_2) \int_0^{\infty} (q_{\lambda_1})_{net} \beta_{\lambda_1} F_{t1}(\lambda_1) d\lambda_1 ,$$

where $\Phi(P,T)$ is the luminescent quantum yield that depends on pressure (P) and temperature (T), $E_{\lambda_2}(\lambda_2)$ is the luminescent emission spectrum, and $F_{t1}(\lambda_1)$ is a filter function describing the optical filter used to insure the excitation light within the absorption spectrum of the luminescent molecules. The boundary condition for (A10) is $I^-_{\lambda_2}(z=h)=0$. The solution to Eq. (A10) is

$$I^-_{\lambda_2} = exp(-\frac{\beta_{\lambda_2} z}{\mu}) \frac{1}{\mu} \left[\int_0^z S_{\lambda_2}(z) exp(\frac{\beta_{\lambda_2} z}{\mu}) dz - \int_0^h S_{\lambda_2}(z) exp(\frac{\beta_{\lambda_2} z}{\mu}) dz \right]. \quad (-1 \le \mu \le 0) \quad \text{(A11)}$$

The incoming luminescent flux toward the wall at the surface (integrated over $\theta = \pi \text{ to } \pi/2$ and $\theta = \pi \text{ to } 3\pi/2$) is

$$q^-_{\lambda_2}(z=0) = -2 \int_{-1}^{0} I^-_{\lambda_2}(z=0) \mu \, d\mu , \qquad \text{(A12)}$$

where

$$I^-_{\lambda_2}(z=0) = -\frac{1}{\mu} \int_0^h S_{\lambda_2}(z) exp(\frac{\beta_{\lambda_2} z}{\mu}) dz .$$

Consider the luminescent emission in the outward direction and assume that the scattering occurs only at the wall. The outgoing luminescent intensity $I^+_{\lambda_2}$ can be described by

$$\mu \frac{d I^+_{\lambda_2}}{dz} + \beta_{\lambda_2} I^+_{\lambda_2} = S_{\lambda_2}(z). \quad (0 \le \mu \le 1) \qquad \text{(A13)}$$

Similar to the boundary condition for the scattering excitation light, we assume that a fraction of the incoming luminescent flux $q^-_{\lambda_2}(z=0)$ is reflected diffusely from the wall. Thus, the boundary condition for Eq. (A13) is

$$I^{+}_{\lambda_2}(z=0) = \rho^{wp}_{\lambda_2}\, q^{-}_{\lambda_2}(z=0) = -2\,\rho^{wp}_{\lambda_2}\int_{-1}^{0} I^{-}_{\lambda_2}(z=0)\,\mu\, d\mu\,, \tag{A14}$$

where $\rho^{wp}_{\lambda_2}$ is the reflectivity of the wall-PSP interface for the luminescent light. The solution to Eq. (A13) is

$$I^{+}_{\lambda_2} = exp(-\frac{\beta_{\lambda_2} z}{\mu})\left[\frac{1}{\mu}\int_0^z S_{\lambda_2}(z)\,exp(\frac{\beta_{\lambda_2} z}{\mu})dz + I^{+}_{\lambda_2}(z=0)\right]. \quad (-1 \le \mu \le 0) \tag{A15}$$

At this stage, the outgoing luminescent intensity $I^{+}_{\lambda_2}$ can be readily calculated by substituting the source term into Eq. A(15). In general, $I^{+}_{\lambda_2}$ has a non-linear distribution across the PSP layer, which is composed of exponentials of $\beta_{\lambda_1} z$ and $\beta_{\lambda_2} z$. For simplicity of algebra, we consider an asymptotic but important case — an optically thin PSP layer. Uncertainty analyses for optically thin and thick PSP layers are essentially the same.

When the PSP layer is optically thin ($\beta_{\lambda_1} h$, $\beta_{\lambda_2} h$, $\beta_{\lambda_1} z$ and $\beta_{\lambda_2} z$ $<<1$), the asymptotic expression for $I^{+}_{\lambda_2}$ is simply

$$I^{+}_{\lambda_2}(z) = \Phi(P,T)\,q_0\,E_{\lambda_2}(\lambda_2)K_1(\beta_{\lambda_1}/\mu)(z + 2\,\rho^{wp}_{\lambda_2} h\,\mu), \qquad (-1 \le \mu \le 0) \tag{A16}$$

where

$$K_1 = \beta^{-1}_{\lambda_1}\int_0^{\infty} \beta_{\lambda_1} E_{\lambda_1}(\lambda_1) C_d (1-\rho^{ap}_{\lambda_1})(1+\rho^{wp}_{\lambda_1}) F_{t1}(\lambda_1)\, d\lambda_1.$$

Eq. (A16) indicates that for an optically thin PSP layer the outgoing luminescent intensity is proportional to the extinction coefficient (the molar absorptivity and luminescent molecule concentration), paint layer thickness, quantum yield of luminescent molecules, and incident excitation light flux. The term K_1 represents the combined effect of the optical filter, excitation

light scattering, and direction of the incident excitation light. The outgoing luminescent intensity averaged over the layer is

$$< I^+_{\lambda_2} > = h^{-1} \int_0^h I^+_{\lambda_2}(z)dz = h\,\Phi(P,T)q_0\, E_{\lambda_2}(\lambda_2)K_1(\beta_{\lambda_1}/\mu)M(\mu), \tag{A17}$$

where $M(\mu) = 0.5 + 2\rho^{wp}_{\lambda_2}\mu$. The outgoing luminescent energy flow rate $Q^+_{\lambda_2}$ on an area element A_s of the PSP paint surface is

$$Q^+_{\lambda_2} = A_s \int_\Omega < I^+_{\lambda_2} > \cos\theta\, d\Omega = \beta_{\lambda_1} h\,\Phi(P,T)q_0\, E_{\lambda_2}(\lambda_2)\, K_1 < M > A_s\Omega\,, \tag{A18}$$

where the unit of $Q^+_{\lambda_2}$ is energy/time/wavelength, Ω is the solid angle, and the extinction coefficient $\beta_{\lambda_1} = \varepsilon_{\lambda_1} c$ is a product of the molar absorptivity ε_{λ_1} and luminescent molecule concentration c. The coefficient $< M >$ represents the effects of reflection and scattering of the luminescent light at the wall, which is defined as

$$< M > = \Omega^{-1} \int_\Omega M(\mu)\, d\Omega = 0.5 + \rho^{wp}_{\lambda_2}(\mu_1 + \mu_2)\,,$$

where $\mu_1 = \cos\theta_1$ and $\mu_2 = \cos\theta_2$ are the cosines of two polar angles in Ω.

Photodetetor output

Consider an optical system located at a distance R_1 from a source area (see Fig. 2). The solid angle with which the lens is seen from the source can be approximated by $\Omega \approx A_0 / R_1^2$, where $A_0 = \pi D^2/4$ is the imaging system entrance aperture area, and D is the effective diameter of the aperture. Using Eq. (A18) and additional relations $A_s / R_1^2 = A_I / R_2^2$ and $1/R_1 + 1/R_2 = 1/fl$, we obtain the energy flux onto the detector

$$(Q_{\lambda_2})_{det} = \frac{\pi}{4} \frac{A_I \, \tau_{op} \, \tau_{atm}}{F^2 (1 + M_{op})^2} \beta_{\lambda_1} h\eta(P,T) q_0 \, E_{\lambda_2}(\lambda_2) \, K_1 < M >, \tag{A19}$$

where $F = fl / D$ is the f-number, $M_{op} = R_2 / R_1$ is the optical magnification, fl is the system's effective focal length, A_I is the image area, and τ_{op} and τ_{atm} are the system's optical transmittance and atmospheric transmittance, respectively. The output of the detector is

$$V = G \int_0^\infty R_q(\lambda_2)(Q_{\lambda_2})_{det} \, F_{t2}(\lambda_2) d\lambda_2 , \tag{A20}$$

where $R_q(\lambda_2)$ is the detector's quantum efficiency, G is the system's gain, and $F_{t2}(\lambda_2)$ is a filter function describing the optical filter for the luminescent emission. The dimension of *V/G* is [*V/G*] = *J/s*. Substitution of Eq. (A19) into Eq. (A20) yields

$$V = G \frac{\pi}{4} \frac{A_I}{F^2 (1 + M_{op})^2} \beta_{\lambda_1} h\Phi(P,T) q_0 \, K_1 \, K_2 \tag{A21}$$

where

$$K_2 = \int_0^\infty \tau_{op} \, \tau_{atm} \, E_{\lambda_2}(\lambda_2) < M > R_q(\lambda_2) F_{t2}(\lambda_2) d\lambda_2 .$$

The term K_2 represents the combined effect of the optical filter, luminescent light scattering, and system response to the luminescent light.

Table I. Sensitivity Coefficients, Elemental Errors, and Total Uncertainty

	Variable ζ_i	Sensitivity Coefficient S_i	Elemental Variance $var(\zeta_i)$	Physical Origin
1	$D_t(\Delta t)$	$\varphi = 1 + \frac{A(T)}{B(T)}\frac{P_{ref}}{P}$	$[(\partial V/\partial t)(\Delta t)/V]^2$	Temporal variation in luminescence due to photodegradation and surface contamination
2	$D_x(\Delta \boldsymbol{x})$	φ	$[(\partial V/\partial x)^2\sigma_x^2 + (\partial V/\partial y)^2\sigma_y^2]V^{-2}$	Image registration errors for correcting luminescence variation due to model motion
3	$D_{q0}(\Delta t)$	φ	$[(\partial q_0/\partial t)(\Delta t)/q_{0\,ref}]^2$	Temporal variation in illumination
4	V_{ref}	φ	$V_{ref}G\hbar\nu B_d$	Photodetector noise
5	V	$-\varphi$	$VG\hbar\nu B_d$	Photodetector noise
6	$\Pi_c/\Pi_{c\,ref}$	φ	$[R_2/(R_1+R_2)]^2(\Delta R_1/R_1)^2$	Change in camera performance parameters due to model motion
7	$\Pi_f/\Pi_{f\,ref}$	φ	$var(\Pi_f/\Pi_{f\,ref})$	Illumination spectral variability and filter spectral leakage
8	h/h_{ref}	φ	$[(\partial h/\partial x)^2\sigma_x^2 + (\partial h/\partial y)^2\sigma_y^2]h_{ref}^{-2}$	Image registration errors for correcting thickness variation due to model motion
9	c/c_{ref}	φ	$[(\partial c/\partial x)^2\sigma_x^2 + (\partial c/\partial y)^2\sigma_y^2]c_{ref}^{-2}$	Image registration errors for correcting concentration variation due to model motion
10	$q_0/q_{0\,ref}$	φ	$(q_{0\,ref})^{-2}\lvert(\nabla q_0)\bullet(\Delta \boldsymbol{X})\rvert^2$	Illumination variation on model surface due to model motion
11	P_{ref}	1	$var(P)$	Error in measurement of reference pressure
12	T	$-\frac{T}{B(T)}[B'(T)+A'(T)\frac{P_{ref}}{P}]$	$var(T)$	Temperature effects of PSP
13	A	$1-\varphi$	$var(A)$	Paint calibration error
14	B	-1	$var(B)$	Paint calibration error
15	Pressure mapping	1	$(\partial P/\partial x)^2\sigma_x^2 + (\partial P/\partial y)^2\sigma_y^2$ and $\lvert(\nabla P)_{surf}\bullet(\Delta \boldsymbol{X})_{surf}\rvert^2$	Errors in camera calibration and pressure mapping on a surface of a presumed rigid body
Total Uncertainty in Pressure			$var(P)/P^2 = \sum_{i=1}^{M} S_i^2\, var(\zeta_i)/\zeta_i^2$	

Note: σ_x and σ_y are the standard deviations of least-squares estimation in the image registration or camera calibration.

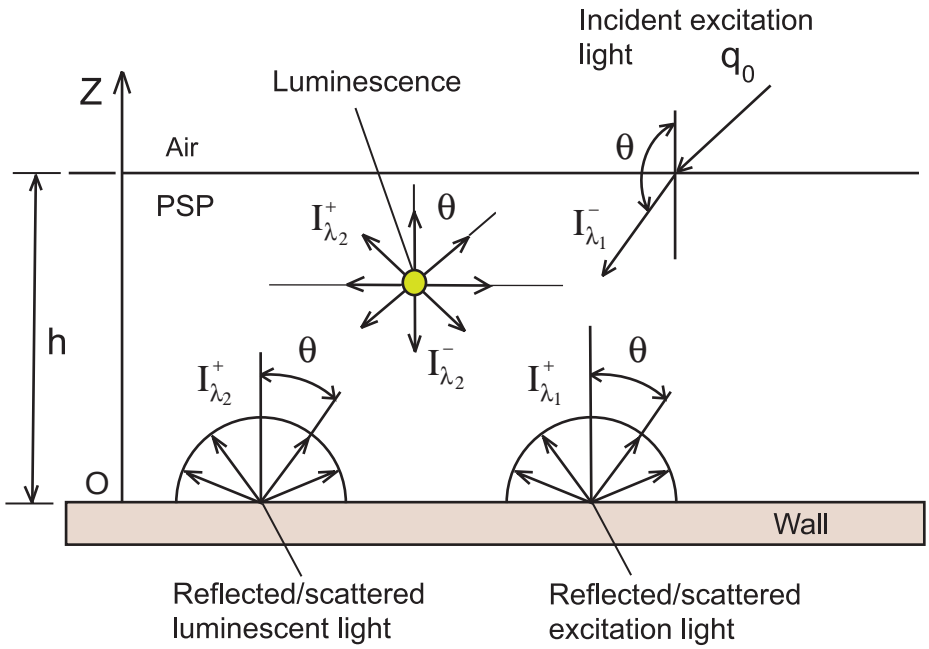

Figure 1. Radiative energy transport processes in PSP.

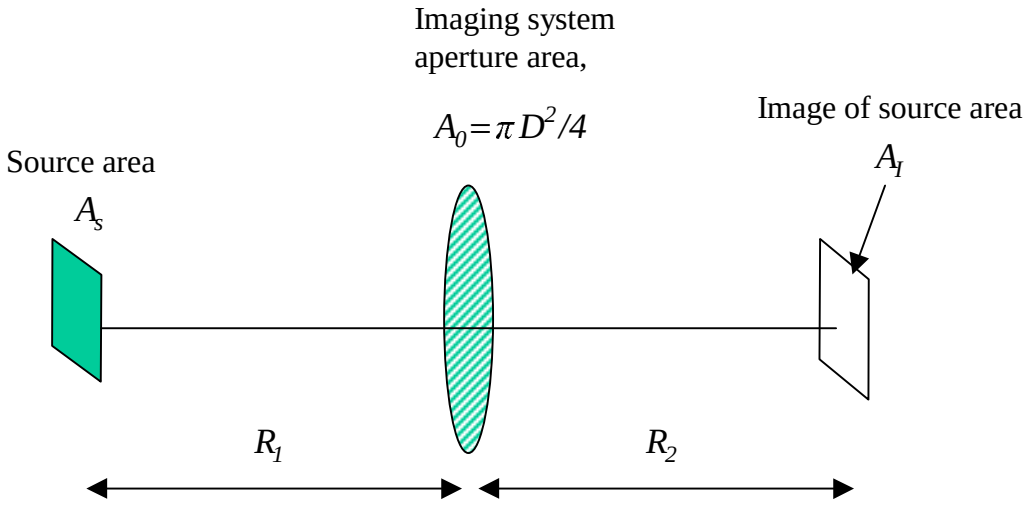

Figure 2. An imaging system.

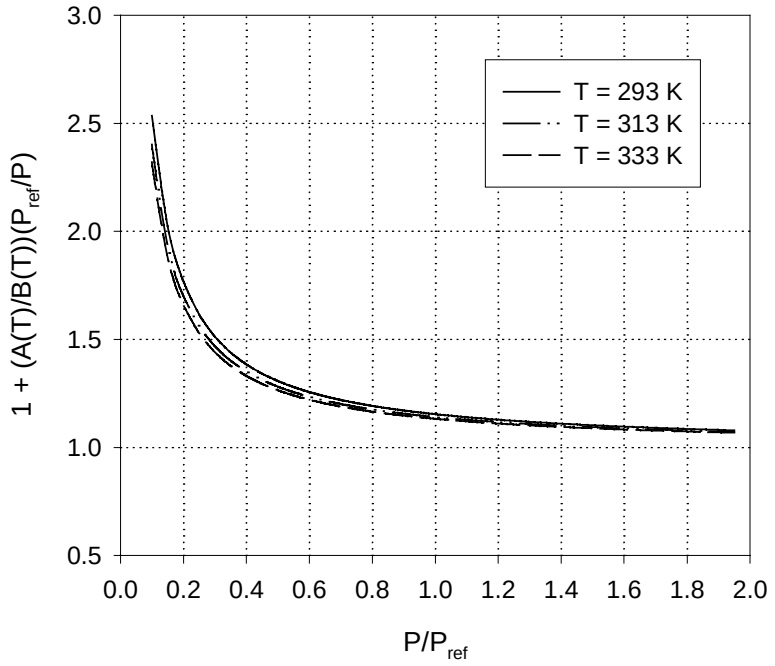

Figure 3. The sensitivity factor $1 + [A(T)/B(T)] / (P/P_{ref})$ as a function of P/P_{ref} at different temperatures for Bath Ruth + silica-gel in GE RTV 118.

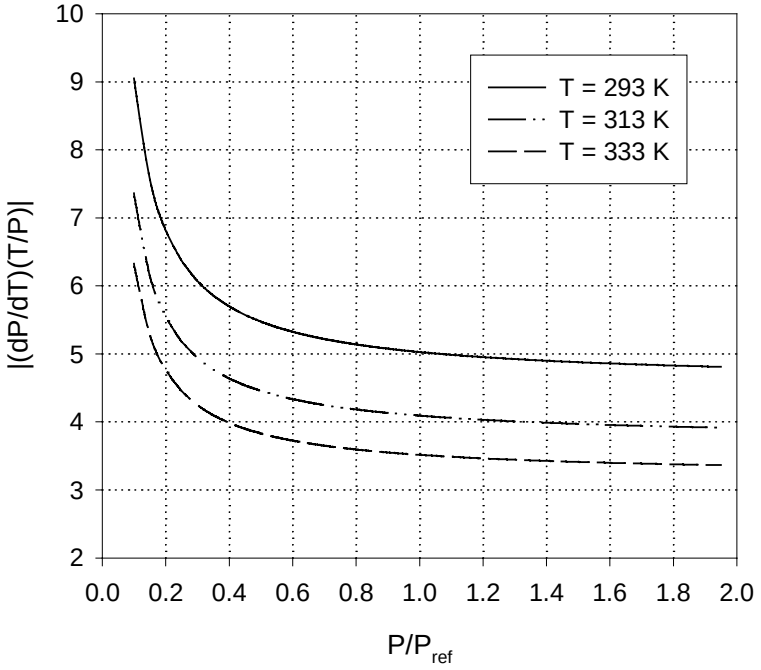

Figure 4. The temperature sensitivity coefficient as a function of P/P_{ref} at different temperatures for Bath Ruth + silica-gel in GE RTV 118.

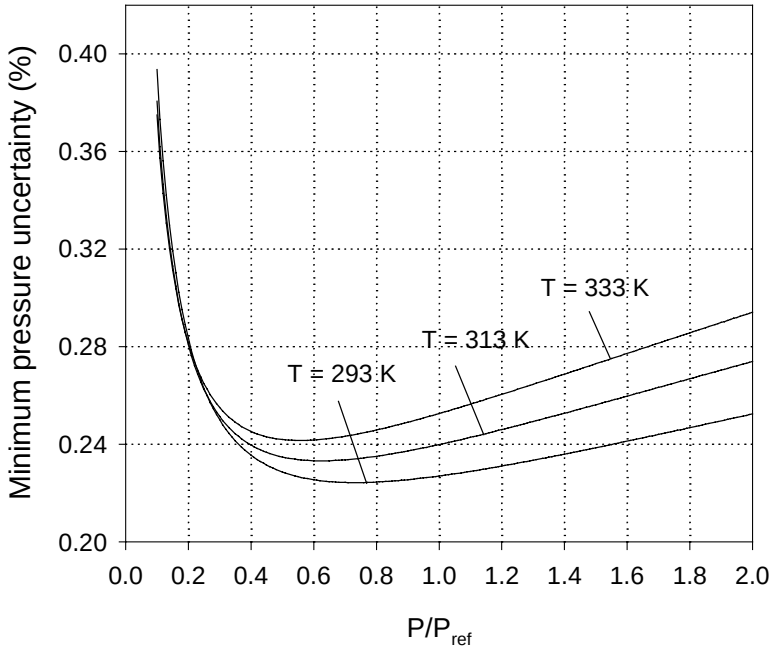

Figure 5. The minimum pressure uncertainty $(\Delta P)_{min} / P$ as a function of P/P_{ref} at different temperatures for Bath Ruth + silica-gel in GE RTV 118.

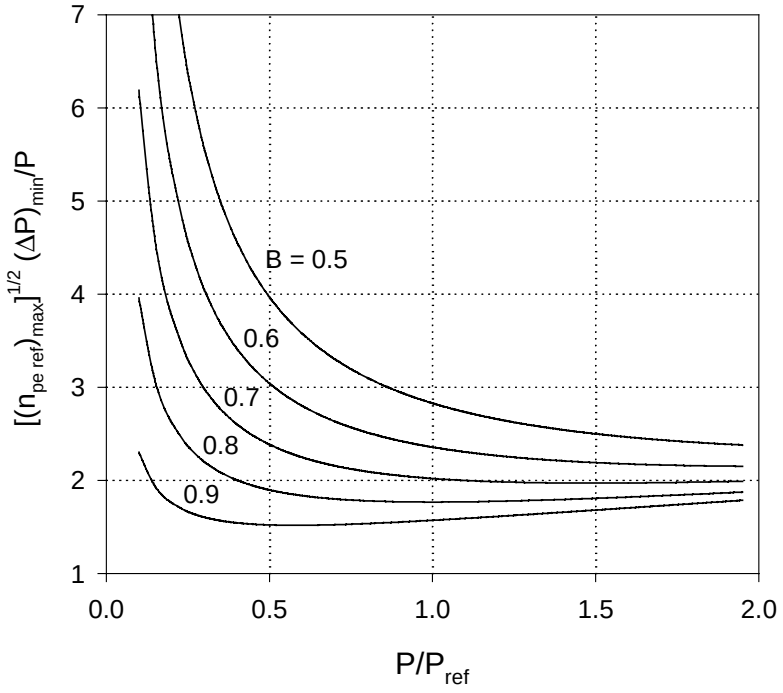

Figure 6. The normalized minimum pressure uncertainty $\sqrt{(n_{pe\,ref}\,)_{max}}\,(\Delta P)_{min}\,/\,P$ as a function of P/P_{ref} for different values of $B(T)$.

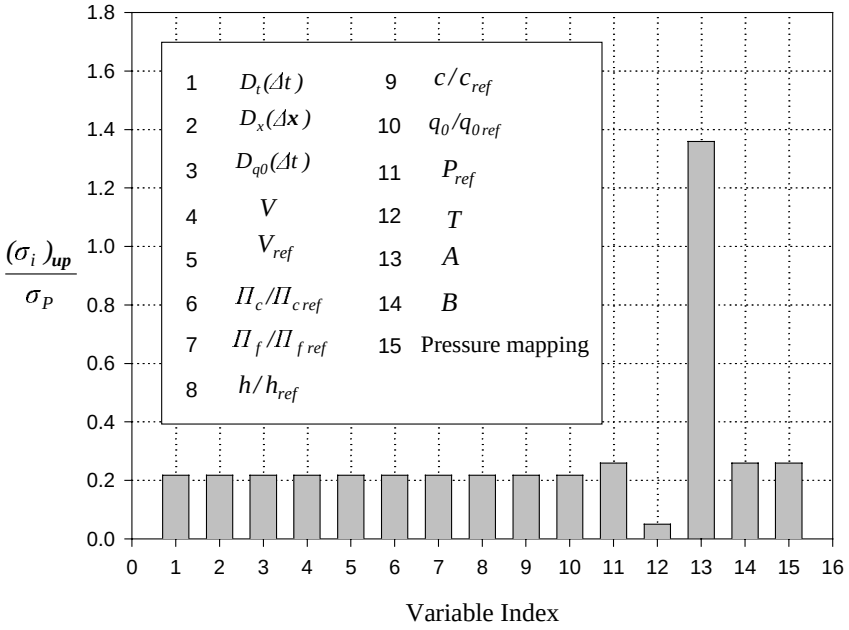

Figure 7. The allowable upper bounds of 15 variables for Bath Ruth + silica-gel in GE RTV 118 when $P / P_{ref} = 0.8$, and $T = 293K$.

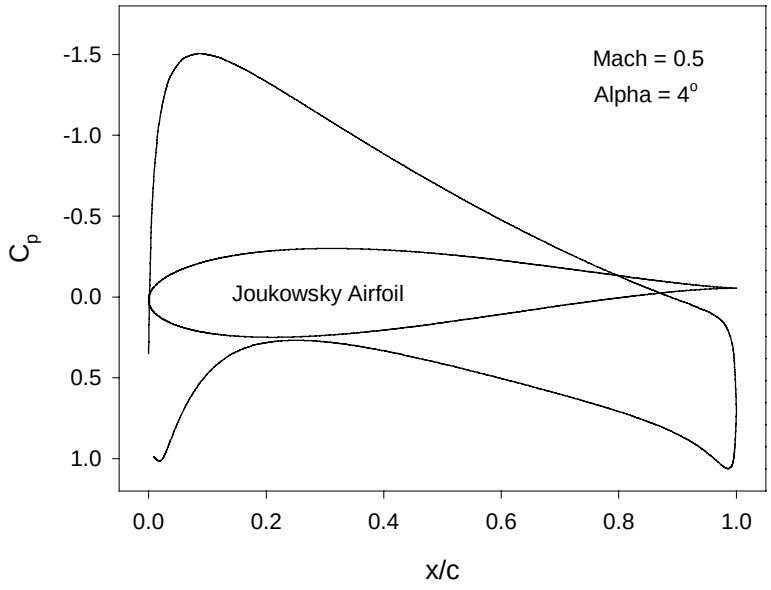

(a)

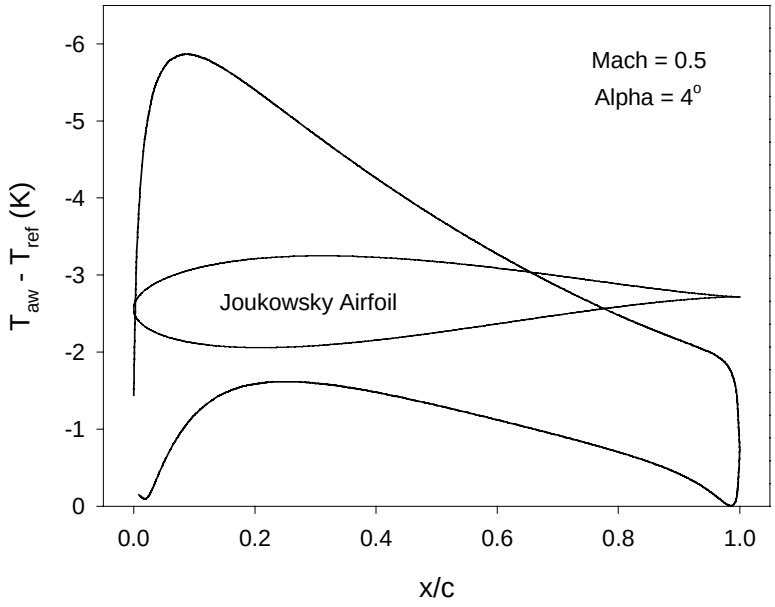

(b)

Figure 8. The pressure coefficient distribution and the adiabatic wall temperature distribution on a Joukowsky airfoil for Mach 0.5 and $T_{ref} = 293K$.

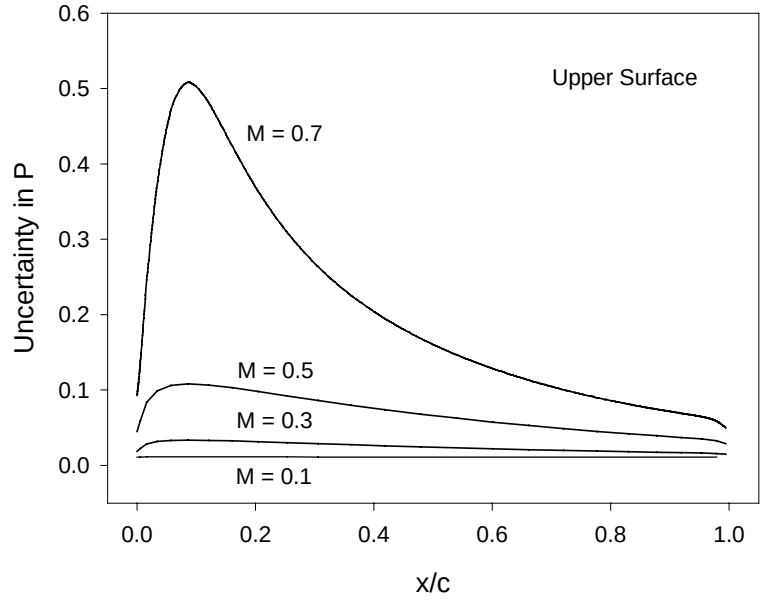

(a)

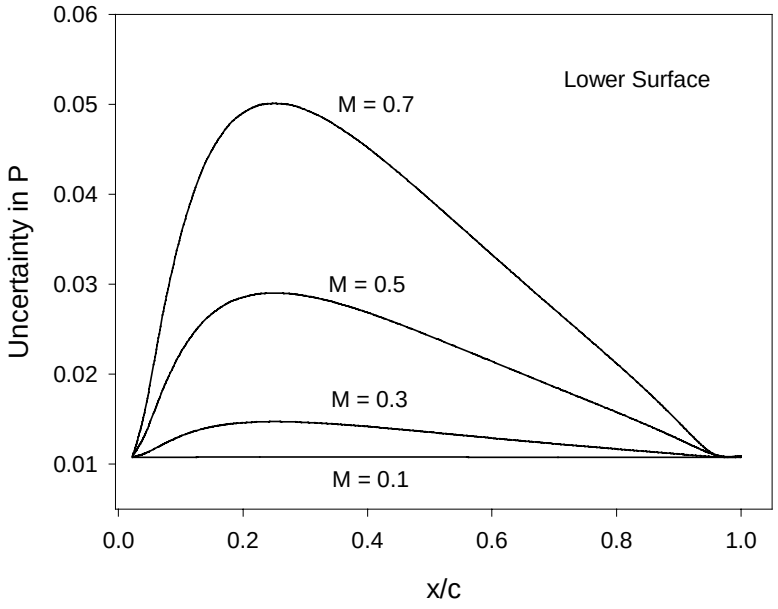

(b)

Figure 9. The PSP uncertainty distributions for different freestream Mach numbers on (a) the upper surface and (b) lower surface of a Joukowsky airfoil.

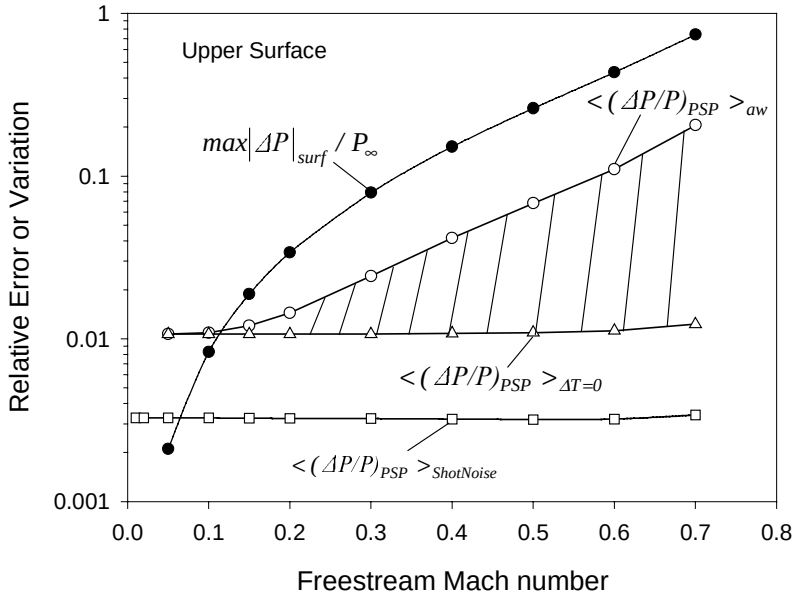

(a)

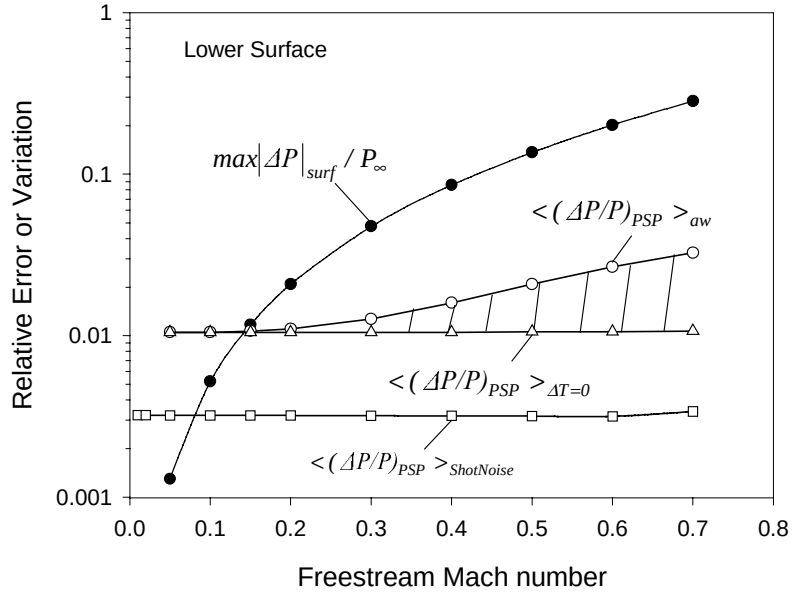

(b)

Figure 10. The maximum relative pressure change and chord-averaged PSP uncertainties as a function of freestream Mach number on (a) the upper surface and (b) the lower surface of a Joukowsky airfoil.

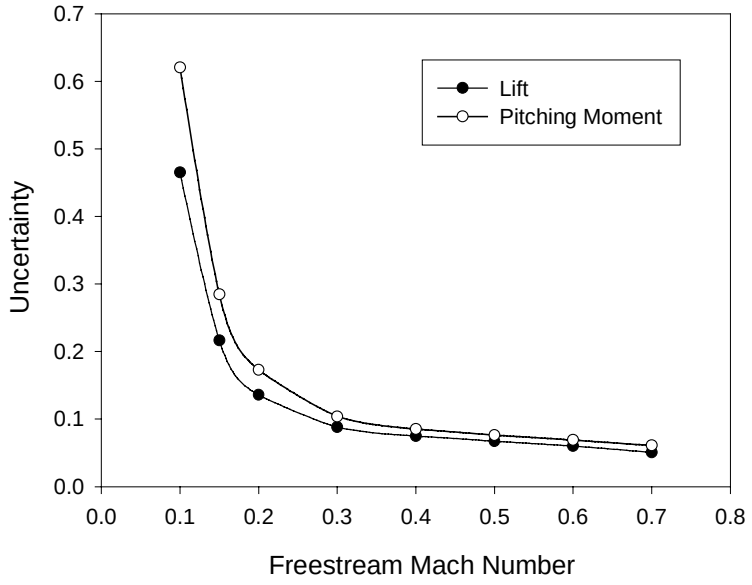

Figure 11. The uncertainties in the lift and pitching moment of a Joukowsky airfoil as a function of freestream Mach number.